Hindawi
International Journal of Energy Research
Volume 2023, Article ID 5512034, 14 pages
https://doi.org/10.1155/2023/5512034

Research Article

Strategies for the High Average *zT* in the Electron-Doped SnTe

Hyunjin Park[1], **Kyu Hyoung Lee**[2], **Minsu Heo**[1], **Sang-il Kim**[1] and **Hyun-Sik Kim**[1]

[1]*Department of Materials Science and Engineering, University of Seoul, 163 Seoulsiripdae-ro, Dongdaemun-gu, Seoul 02504, Republic of Korea*
[2]*Department of Materials Science and Engineering, Yonsei University, 50 Yonsei-ro, Seodaemun-gu, Seoul 03722, Republic of Korea*

Correspondence should be addressed to Sang-il Kim; sang1.kim@uos.ac.kr and Hyun-Sik Kim; hyunsik.kim@uos.ac.kr

Received 9 August 2023; Revised 10 October 2023; Accepted 24 November 2023; Published 15 December 2023

Academic Editor: Raja Sen

We propose a new strategy to achieve a high average *zT* in electron-doped SnTe by applying the two-band (TB) and single parabolic band (SPB) models to the electronic transport properties of $Sn_{0.97}M_{0.03}Te$ (M = Ga, In, Bi, and Sb) reported in the literature. To achieve a high average *zT* at temperatures from 300 to 823 K, both *zT* at 300 and 823 K should be high with a steadily increasing *zT* over the temperatures. The *p*-type SnTe is known to have a light valence band and a heavy valence band that are approximately 0.40 eV apart. The Bi-doped SnTe exhibits one of the highest *zT* among all the other doped samples at 300 K (0.09) and the highest *zT* at 823 K (0.9), with a steadily increasing *zT* in between. The TB model confirms the presence of the resonant state at 300 K which is responsible for the high *zT* at 300 K. The *B*-factor, which is related to the theoretical maximum *zT*, calculated by the SPB model indicates a steady increase in *zT* with increasing temperature. The temperature-dependent *B*-factor of the Bi-doped SnTe suggests that the initial position of its Fermi level at 300 K calculated by the TB model may be responsible for the temperature coefficient of the *B*-factor, which determines the *zT* at 823 K. According to the SPB model, experimental *zT* of 0.9 of the Bi-doped SnTe can be further improved to 1.03 (14% improvement) at 823 K upon carrier concentration optimization. To achieve a high average *zT* in SnTe, electron doping with a dopant that forms a resonant state and placing the Fermi level at the light valence band in the vicinity of the heavy valence band maximum are both essential.

1. Introduction

Efforts to prevent accelerating global warming are continuing through research on various sustainable energy harvesting technologies. They have made significant contributions to reducing greenhouse gas emissions, which are the primary cause of global warming [1]. Thermoelectric technology, one of the environmentally friendly energy harvesting technologies, is attracting much attention as it can generate electricity directly from waste heat without combusting fossil fuels [2]. The current efficiency of thermoelectric power generation devices is not yet high enough to compete with conventional coal-fired power plants. The efficiency of thermoelectric devices is closely linked to the thermoelectric figure-of-merit (*zT*) of the materials used in the devices. As a result, many studies have focused on increasing the *zT* of thermoelectric materials. The zT ($=S^2\sigma T/\kappa$) depends on the Seebeck coefficient (S), electrical conductivity (σ), temperature (T in Kelvin), and thermal conductivity (κ). The κ is, in turn, a sum of electronic contribution to thermal conductivity (κ_e) and lattice thermal conductivity (κ_l) [2, 3]. The $S^2\sigma$ in zT is called the power factor (*PF*), and it determines the electron transport properties of the material. As shown in the zT equation, the zT is maximized when the *PF* is high and the κ is low.

However, it is difficult to increase the *PF* because the S and σ of the material have a trade-off relationship with a changing Hall carrier concentration (n_H) [2, 4–6]. For example, as the n_H increases, the σ of a material increases while its S decreases. For this reason, the *PF* of a thermoelectric material peaks at a specific n_H, and optimizing the n_H for the highest *PF* is an important goal in thermoelectric research. In addition, many band engineering strategies have been

shown to be effective in improving the *PF* by bypassing the trade-off between the *S* and σ. For example, the band convergence strategy increases the number of the Fermi pockets (valley degeneracy) of electronic bands that contribute mainly to electronic transport by aligning two bands similar in energy. When two bands approach each other in energy, the density-of-state effective mass (m_d^*) increases, leading to an enhancement of the *S* without a decrease σ. This increase in m_d^* is due to the increase in the number of the Fermi pockets, which does not lead to a decrease in σ [7–9]. The κ_l is the only parameter in the zT equation that can be lowered without significantly affecting other parameters in zT. The κ_l reduction can be achieved through complex crystal structuring and nano-/meso- or all-scale architecturing [10, 11].

Chalcogenides that include Bi, Sb, Sn, or Ge elements are currently the most promising materials for thermoelectric applications. Among these materials, SnTe has recently emerged as a popular choice in the development of clean energy sources due to its Pb-free composition [12–14]. Although SnTe has a crystal structure and electronic structure similar to that of PbTe, its zT is lower than that of PbTe due to its high intrinsic defect concentrations, narrow bandgap, and high energy difference between the highest and the 2nd highest valence bands [14]. Banik et al. demonstrated that Mg alloying in SnTe significantly improved the *S* because of the reduction in the energy difference between the highest valence band (light valence band) and the 2nd highest valence band (heavy valence band) [15]. The energy difference between the light valence band and the heavy valence band is approximately 0.40 eV at room temperature [14]. Tan et al. reported that Hg alloying in SnTe increased the bandgap and decreased the energy difference between the light and heavy valence bands, simultaneously. In other words, Hg alloying promotes band convergence while suppressing bipolar conduction [16]. Tan et al. showed that Mn alloying in SnTe tuned the valence bands and exhibited an *S* higher than expected from the band convergence between the light and heavy valence bands [17]. Recently, Zhao et al. reported a high zT of 0.9 at 823 K in Bi-doped SnTe ($Sn_{0.97}Bi_{0.03}Te$) [14]. This was achieved by electron doping with Bi, which effectively maximized the electronic transport properties of SnTe. The experimental *S* and n_H of the Bi-doped SnTe coincided with the highest *S* ($\sim 53\,\mu V\,K^{-1}$) at the optimum n_H ($\sim 2 \times 10^{20}\,cm^{-3}$) calculated using the two-band (TB) model at 300 K. Other dopants (Ga, In, and Sb) also decreased the n_H of SnTe, but it was the Bi dopant that optimized the n_H for the highest *S* in $Sn_{0.97}M_{0.03}Te$ (*M* = Ga, In, Bi, and Sb). However, the advantages of Bi doping in SnTe relative to other dopants (Ga, In, and Sb) were not fully explored. The potential impact of resonant state formation via Bi doping was also not considered.

In this study, we first evaluated the effect of electron doping (Ga, In, Bi, and Sb) on SnTe using the TB model, which considers one light valence band and one heavy valence band. By comparing the Seebeck–Pisarenko (*S* vs. n_H) calculated via the TB model and the experimental data of $Sn_{0.97}M_{0.03}Te$ (*M* = Ga, In, Bi, and Sb), we found that the Bi-doped SnTe generated a resonant state on top of electron doping. Once we confirmed the resonant state formation via Bi doping, we then performed the single parabolic band (SPB) model calculations for $Sn_{0.97}M_{0.03}Te$ (*M* = Ga, In, Bi, and Sb) to evaluate how different electron doping affects the electronic band parameters when a single parabolic band was assumed. The reason that we first employed the TB model instead of the SPB model was that the SPB model could only provide the information about the density-of-states effective mass (m_d^*) change, but not the reason behind it. We calculated the temperature-dependent m_d^*, nondegenerate mobility (μ_0), weighted mobility (μ_W), and *B*-factor of $Sn_{0.97}M_{0.03}Te$ (*M* = Ga, In, Bi, and Sb) using the SPB model [18]. From the temperature-dependent band parameters, we analyzed the reason behind the high zT of Bi-doped SnTe at high temperatures (~823 K). We found that the resonant state formation and temperature coefficient of *B*-factor are responsible for the high zT (~0.9) of $Sn_{0.97}Bi_{0.03}Te$ at 823 K. The temperature coefficient of the *B*-factor that is favorable to all temperature ranges can be achieved if the Fermi level (η) is placed at the light valence band in the vicinity of the heavy valence band maximum. We also found that the zT of the Bi-doped sample can be improved to 1.03 (14% improvement) if the n_H is tuned to $1.1 \times 10^{20}\,cm^{-3}$. Although the average zT of the Bi-doped sample is the highest among other samples after the n_H optimization, the SPB model shows that the theoretical maximum zT of the Sb-doped sample (1.13) is even higher than that of the Bi-doped sample at 823 K.

2. Method

2.1. SPB Model. The temperature-dependent *S* and n_H of the $Sn_{0.97}M_{0.03}Te$ (*M* = Ga, In, Bi, and Sb) samples were obtained from Zhao et al. [14]. With the SPB model, the *S* is defined as follows [19]:

$$S = \frac{k_B}{e}\left(\eta - \frac{2F_1(\eta)}{F_0(\eta)}\right). \quad (1)$$

The Fermi integral of order j (F_j) in Equation (1) is defined as in Equation (2) [20, 21].

$$F_n(\eta) = \int_0^\infty \frac{\varepsilon^n}{1 + \exp(\varepsilon - \eta)}\, d\varepsilon. \quad (2)$$

The n_H is defined by m_d^* and η as shown in Equation (3) [20, 21].

$$n_H = 16\frac{\pi}{3}\left(\frac{2m_d^* k_B T}{h^2}\right)^{3/2}\frac{(F_0(\eta))^2}{F_{-1/2}(\eta)}. \quad (3)$$

At a consistent temperature, the *S* lines that vary with n_H can be matched to the empirical findings by tuning the m_d^* in Equation (3). The SPB model allows for the anticipation of *S* under varied n_H conditions not explored in the experiments.

The μ_0 was calculated from the experimental n_H-dependent μ_H at different temperatures (from Zhao et al.) using the SPB

model [5, 14]. According to the SPB model under acoustic phonon scattering assumption, the μ_H is defined in terms of the μ_0 and the Fermi level (η) (Equation (4)) [22].

$$\mu_H = \mu_0 \frac{F_{-1/2}(\eta)}{2F_0(\eta)}. \tag{4}$$

The μ_0 was fitted to the experimental n_H-dependent μ_H using Equations (3)–(5).

The μ_W is defined as in Equation (5) [23].

$$\mu_W = \mu_0 \left(\frac{m_d^*}{m_0}\right)^{3/2}. \tag{5}$$

The B-factor is determined from the μ_W, κ_l, and T as shown in Equation (6), where e, h, and k_B are the electric charge, Planck's constant, and Boltzmann's constant, respectively [23].

$$B = \left(\frac{k_B}{e}\right)^2 \frac{8\pi e(2m_0 k_B)^{3/2}}{h^3} \frac{\mu_W T^{5/2}}{\kappa_l}. \tag{6}$$

2.2. TB Model. With the two-band model, the S and σ are defined as in Equations (7) and (8), where the lower subscript L and H mean the light valence band and the heavy valence band [24].

$$S = \frac{S_L\sigma_L + S_H\sigma_H}{\sigma_L + \sigma_H}, \tag{7}$$

$$\sigma = \sigma_L + \sigma_H = p_L\mu_L e + p_H\mu_H e. \tag{8}$$

S_L, the Seebeck coefficient of the light-mass valence band, is defined as in Equation (9) [24].

$$S_L = \frac{k_B}{e}\left[\frac{{}^1F_{-2}^1(\eta)}{{}^0F_{-2}^1(\eta)} - \eta\right], \tag{9}$$

$${}^nF_l^m(\eta) = \int_0^\infty \left(-\frac{\partial f}{\partial \varepsilon}\right)\varepsilon^n\left(\varepsilon + \alpha\varepsilon^2\right)^m\left[(1+2\alpha\varepsilon)^2 + 2\right]^{l/2} d\varepsilon. \tag{10}$$

p_L, the chemical carrier concentration of the light-mass valence band, is defined as in Equation (11) [24].

$$p_L = \frac{(2m^* k_B T)^{3/2}}{3\pi^2\hbar^3}\,{}^0F_0^{3/2}(\eta). \tag{11}$$

A_L, the hall factor of light-mass valence band, is defined as in Equation (12) [24].

$$A_L = \frac{3K(K+2)}{(2K+1)^2}\frac{{}^0F_{-4}^{1/2}(\eta)\,{}^0F_0^{3/2}(\eta)}{\left({}^0F_{-2}^1(\eta)\right)^2}. \tag{12}$$

μ_L, the mobility of light-mass valence band, is defined as in Equation (13) [24].

$$\mu_L = \frac{2\pi\hbar^4 eC_l}{m_d^*(2N_v k_B T)^{3/2}E_{def}^2}\frac{3\,{}^0F_{-2}^1(\eta)}{{}^0F_0^{3/2}(\eta)}. \tag{13}$$

And for the heavy-mass valence band, the Seebeck coefficient (S_H), chemical carrier concentration (p_H), Hall factor (A_H), and mobility (μ_H) are defined as follows [24, 25]:

$$\begin{aligned} S_H &= \frac{k_B}{e}\left[\frac{{}^1F_{-2}^1(\eta-\Delta)}{{}^0F_{-2}^1(\eta-\Delta)} - (\eta-\Delta)\right], \\ \Delta &= \frac{E_v}{k_B T}, \\ p_H &= \frac{(2m^* k_B T)^{3/2}}{3\pi^2\hbar^3}\,{}^0F_0^{3/2}(\eta-\Delta), \\ A_H &= \frac{3}{2}F_{1/2}\frac{F_{-1/2}}{2F_0^2}, \\ \mu_H &= R_H\sigma, \end{aligned} \tag{14}$$

where R_H is the hall coefficient [25],

$$R_H = \frac{\sigma_L^2 R_{\mathrm{HL}} + \sigma_H^2 R_{\mathrm{HH}}}{(\sigma_L + \sigma_H)^2}. \tag{15}$$

Table 1 shows the band parameters that we used in this study [24, 25].

3. Results and Discussion

Figure 1(a) shows the experimental n_H-dependent S of the pristine and electron-doped (Ga, In, Bi, and Sb) SnTe. The measurements from Zhao et al. are presented with filled symbols [14], while those from other literature are presented with empty symbols [16, 26–28]. The solid line in Figure 1(a) is the n_H-dependent S calculated for the pristine SnTe using the TB model (1 light valence band + 1 heavy valence band). The light valence band (LVB) is 0.18 eV apart from the lowest conduction band edge, and it is approximately 0.38 eV higher than the heavy valence band (HVB). For the $m_d{}^*$ of LVB and HVB, 0.13 m_0 and 1.92 m_0 are used, respectively. Considering the narrow band gap (E_g) between the LVB and the conduction band minimum, LVB is set to be nonparabolic (with the band nonparabolicity parameter of $0.14 = k_B T/E_g$ at 300 K). For simplicity, the HVB with E_g of 0.56 eV (0.18 + 0.38 eV) is assumed parabolic. These details of SnTe band structure incorporated in the TB model closely follow those adopted by Zhang et al. [24] (Table 1).

The n_H-dependent S calculated by the TB model (dark grey solid line in Figure 1(a)) decreases until $\sim 1.3 \times 10^{20}$ cm^{-3} (shaded in blue) and suddenly peaks at around 6.2×10^{20} c m^{-3}. The abrupt increase in the S for n_H in the range from 1.3×10^{20} cm^{-3} to 6.2×10^{20} cm^{-3} (shaded in light blue) is closely related to the presence of the HVB 0.38 eV below the LVB. As the n_H increases the Fermi level at the LVB enters a regime where contribution from HVB becomes significant. However, the Fermi level that corresponds to the local

Table 1: Band parameters of the light and heavy bands in SnTe.

Band parameter	Value
C_l	5.82×10^{10} kg s^{-2} m^{-1}
κ_l	1.917 Wm^{-1} K^{-1}
$m_L{}^*$	0.125 m_0
$m_H{}^*$	1.92 m_0
$N_{v,L}$	4
$N_{v,H}$	12
$E_{\mathrm{def},L}$	40 eV
$E_{\mathrm{def},H}$	25 eV

maximum S (33 μV K^{-1}) at 6×10^{20} cm^{-3} is not exactly at the HVB maximum. The blue-shaded and light blue-shaded regions in Figure 1(a) are translated in terms of Fermi levels in Figure 1(c).

Electron doping is effective in decreasing the n_H of SnTe. According to the pristine SnTe and $Sn_{0.97}M_{0.03}Te$ (M = Ga, In, Bi, and Sb) samples (filled symbols) in Figure 1(a), the experimental n_H of $Sn_{0.97}M_{0.03}Te$ (M = Ga, In, Bi, and Sb) samples are all lower than that of SnTe (1.27×10^{21} cm^{-3}). The n_H of the $Sn_{0.97}Ga_{0.03}Te$ sample is in the region where the HVB is dominant (no shading). The n_H of the $Sn_{0.97}In_{0.03}Te$ and $Sn_{0.97}Bi_{0.03}Te$ samples are in the region where both HVB and LVB contribute to electronic transport (shaded in light blue). The n_H of the $Sn_{0.97}Sb_{0.03}Te$ sample is in the region where only LVB is dominant (shaded in blue). While the n_H-dependent S measurements for the pristine SnTe, $Sn_{0.97}Ga_{0.03}Te$, and $Sn_{0.97}Sb_{0.03}Te$ can be described with the TB model calculation results (solid line), those for $Sn_{0.97}In_{0.03}Te$ and $Sn_{0.97}Bi_{0.03}Te$ are deviated from the TB model significantly. It is well known that In doping in SnTe generates resonant state within the valence band which causes an increase in S higher than expected from the TB model [24]. However, the formation of resonant states via Bi doping is not well understood, as experimental results have been contradictory. For example, the Bi-doped SnTe measurements reported by Vedeneev et al. and Galushchak et al. closely follow the TB model results, which suggests that Bi doping only alters the Fermi level without changing any band parameters of LVB and HVB [27, 28]. However, the experimental S of the Bi-doped SnTe samples from Zhao et al., Tan et al., and Zhou et al. are higher than the TB model prediction at their experimental n_H. This indicates that the Bi doping alters the band structure of SnTe. Possible resonant state formation in SnTe by Bi doping has been proposed recently by Shenoy and Bhat from density functional theory (DFT) calculations [29, 30]. Additionally, we have estimated how the Seebeck–Pisarenko (n_H-dependent S) would change as the energy offset between the LVB and HVB decreases. The Seebeck–Pisarenko lines with energy offset being smaller than 0.38 eV are shown in light grey lines. As the energy offset decreases, the hump near 6.2×10^{20} cm^{-3} (when the energy offset is 0.38 eV) shifts to lower n_H and disappears when the energy offset is zero. Even when the LVB and HVB are converged (light grey dotted line), the experimental data for Bi-doped SnTe (with high Bi doping content) do not agree with the TB model results. Based on the reasons outlined above, it is suggested that resonant state formation is likely to occur in Bi-doped SnTe with high Bi-doping concentrations. Vedeneev et al. doped Bi at a concentration of 1 at.%, while other samples have a Bi doping content of 2 at.% or higher. The amount of Bi doping content, combined with the doping site (Bi can replace either Sn or Te), which may change with the doping content, must have resulted in the contradicting results for the Bi-doped samples as shown in Figure 1(a).

Figure 1(b) shows the experimental n_H-dependent μ_H of the pristine and electron-doped (Ga, In, Bi, and Sb) SnTe (in symbols). Some of the Bi-doped samples (presented in Figure 1(a)), which did not report their μ_H measurements, were omitted in Figure 1(b). The TB model result is shown in the solid line. No abrupt change in the μ_H is observed in the TB model result. The appearance of HVB at high n_H decreases the rate of μ_H decrease with increasing n_H ($>10^{20}$ cm^{-3}). The absence of a hump in the calculated n_H -dependent μ_H (unlike the calculated n_H-dependent S in Figure 1(a)) can be explained by the different electrical conductivity-weighted averaging of the contributions to S and μ_H from the LVB and HVB. It is to be noted that the n_H-dependent μ_H measurements of all the samples have reasonable agreements with the TB model. This includes the In-doped and Bi-doped SnTe samples. If their experimental μ_H are lower than those predicted by the TB model, we cannot claim the formation of resonant state via In or Bi doping. In that case, the S enhancement would be explained with the conventional S-σ trade-off relation. In other words, the experimental n_H-dependent μ_H of the Bi-doped SnTe samples in Figure 1(b) would have lower μ_H than the TB model result at the given n_H if the $m_d{}^*$ of the HVB have become heavier with Bi doping. Because the S enhancement of In or Bi-doped SnTe greater than calculated by the TB model (Figure 1(a)) is not accompanied by corresponding reduction in μ_H (hence σ), and the S enhancement of Bi-doped SnTe cannot be explained by the band convergence between the LVB and HVB (light grey lines in Figure 1(a)), it is very likely that the high experimental S (71 μV K^{-1}) of $Sn_{0.97}Bi_{0.03}Te$ is due to the resonant state formation on top of the electron doping.

Figure 1(c) shows the schematic band structure of the pristine SnTe and the Fermi levels (in unit of k_BT) of the pristine and $Sn_{0.97}M_{0.03}Te$ (M = Ga, In, Bi, and Sb) calculated by the TB model (in dashed lines). The Fermi level (η) of 0 is set to be at the LVB maximum (in yellow). The energy difference (ΔE) between the LVB maximum and HVB maximum (in green) is 14.6 (0.38 eV at 300 K). The blue- and light blue-shaded regions in Figure 1(c) correspond to those shown in Figures 1(a) and 1(b). The only difference is that the shaded regions in Figure 1(c) are expressed in terms of the η and not the n_H. The η is a better indicator of the degeneracy than the n_H, as the n_H can be misleading due to its dependence on $m_d{}^*$. The S decreases with increasing n_H until the η is 11 above the HVB maximum (shaded in blue). However, once

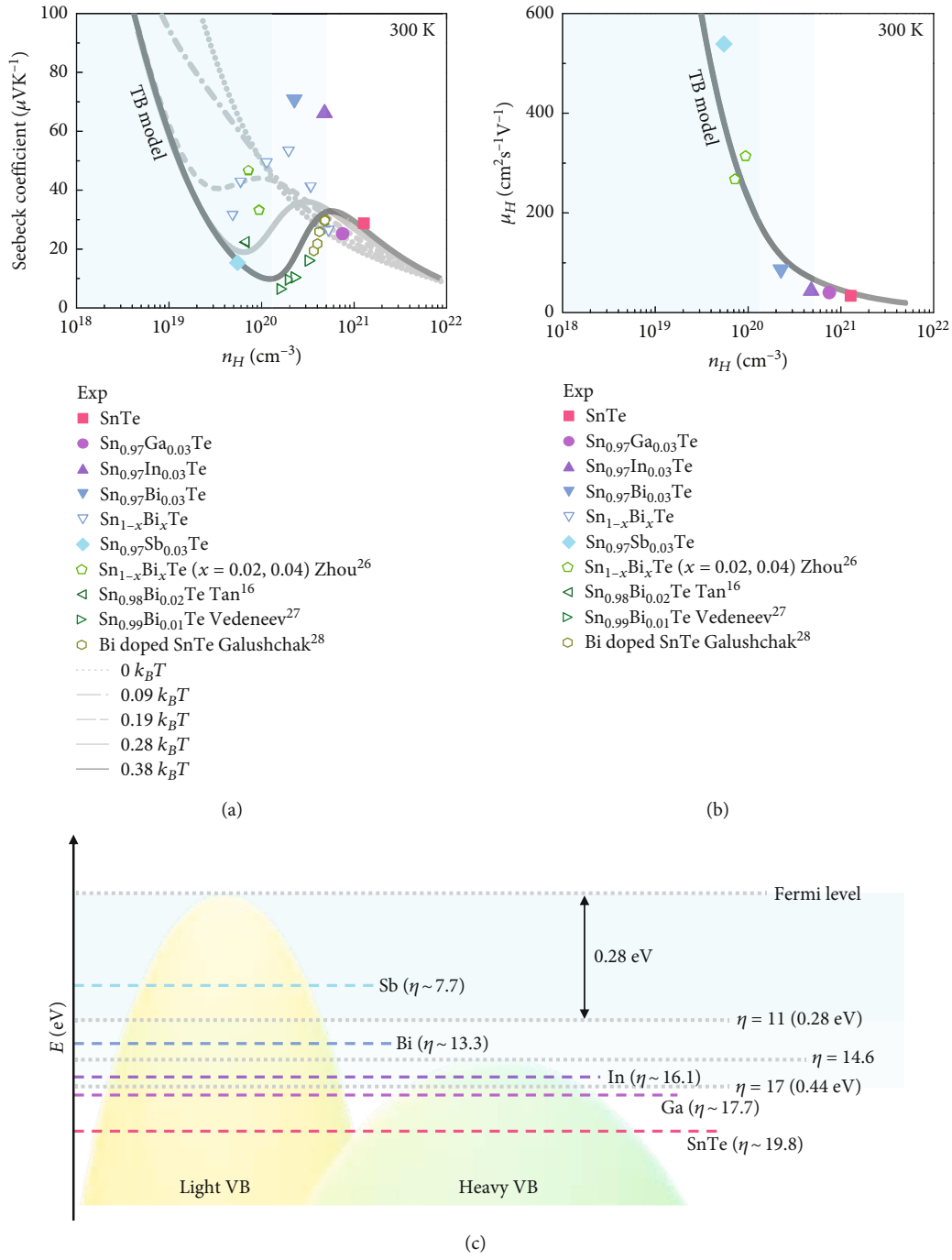

Figure 1: (a) S and (b) μ_H of pristine and electron-doped (Ga, In, Bi, and Sb) SnTe as a function of n_H from the experiments (in symbols) and the TB model calculations (in lines) [14, 16, 26–28]. (c) The Fermi levels (in dashed lines) of pristine SnTe and $Sn_{0.97}M_{0.03}Te$ (M = Ga, In, Bi, and Sb) estimated by the TB model at 300 K [14].

the ΔE between the η and the HVB maximum is smaller than 11, the contribution from the HVB kicks in, and the S improves with an increasing n_H. This continues until the η is 17 below the HVB maximum (shaded in light blue). When the ΔE between the η and the HVB maximum is greater than 17, the contribution from the LVB becomes negligible, and the S decreases again as the n_H increases (no shading). The η of both In-doped and Bi-doped samples are in the region where both LVB and HVB contribute to transport. Resonant state formation and optimally placed Fermi level are the physical reasons behind the high zT of In-doped (zT~0.1) and Bi-doped samples (~0.09) at 300 K. The zT of Bi-doped sample (zT~0.9) becomes higher than the In-doped sample (~0.6) at higher temperatures.

The band structure of SnTe is well-known at 300 K (Figure 1(c)). However, the band structure at high temperatures

is hardly studied, making the TB model calculation of SnTe at high temperatures difficult. Once we confirmed the existence of the resonant state in the In-doped and Bi-doped samples at 300 K using the TB model, we switched the evaluation tool to the single parabolic band (SPB) model, for simplicity. The reason that we switched from the TB model to the SPB model is that the SPB model is simpler and more intuitive than the TB model while capturing important characteristics of the electronic band structures. When electronic transport properties are fitted by the TB model, we need to fit 4 different band parameters (2 effective masses and 2 deformation potentials for the LVB and HVB). In contrast, only two band parameters (1 effective mass and 1 deformation potential) need to be fitted when the SPB model is utilized. Therefore, the effect of resonant state formation and electron doping can be more intuitively understood with the SPB model than with the TB model.

Figure 2(a) shows the experimental and calculated S as a function of n_H at 300 K [14]. By fitting Equations (1) and (3) to the experimental data (in filled symbols), the calculated n_H-dependent S (in lines) are achieved. The pristine SnTe has the highest n_H (1.3×10^{21} cm^{-3}). The n_H decreases as Ga, In, Bi, and Sb are doped to SnTe. The n_H of $Sn_{0.97}Ga_{0.03}Te$ (7.5×10^{20} cm^{-3}) is only 40% smaller than that of SnTe, while the n_H of $Sn_{0.97}Sb_{0.03}Te$ (5.5×10^{19} cm^{-3}) is approximately 95% smaller than that of SnTe. The S of pristine SnTe (~29 μV K^{-1}) decreases to 25 and 17 μV K^{-1}, respectively, as Ga and Sb are doped. However, the S significantly improves when In (66 μV K^{-1}) and Bi (71 μV K^{-1}) are doped into SnTe. From the TB model results (Figure 1), we know that the S improvements in In-doped and Bi-doped samples are due to the resonant state formation and the η appropriately positioned where the HVB starts to contribute to the electronic transport (shaded in light blue in Figure 1(c)).

Figure 2(b) shows the calculated 300 K m_d^* of pristine SnTe and $Sn_{0.97}M_{0.03}Te$ (M = Ga, In, Bi, and Sb) obtained from Figure 2(a). The m_d^* of pristine SnTe is 1.67 m_0 (SPB model). According to the TB model, the m_d^* of the LVB and HVB in SnTe were 0.13 and 1.92 m_0 (Figure 1). The η of SnTe is approximately 5.2 k_BT (~0.13 eV at 300 K) below the HVB maximum (Figure 1(c)). This means that the majority of electronic contributions to SnTe come from the HVB. Consequently, its m_d^* estimated by the SPB model (1.67 m_0) is comparable to the m_d^* of the HVB in the TB model (1.92 m_0). Although the m_d^* in Figure 2(b) is estimated while assuming there is only one parabolic band contributing to transport, it directly corresponds to the actual band structure and the position of its Fermi level we obtained from the TB model (Figure 1(c)). The Sb-doped SnTe which has the lowest m_d^* has its Fermi level positioned at the LVB farthest from the top of the HVB (Figure 1(c)). The m_d^* of $Sn_{0.97}Ga_{0.03}Te$ is 1.03 m_0 (SPB model). The Ga-doped sample has a smaller η (~17.7) than the pristine SnTe (~19.8) in Figure 1(c), meaning that the η is closer to the HVB maximum. This indicates that the LVB is more populated in the Ga-doped sample. When the contributions from the two bands are approximated to that from one band, the effective mass m_d^* is expected to be lighter than that of the pristine SnTe. The m_d^* of $Sn_{0.97}In_{0.03}Te$ and $Sn_{0.97}Bi_{0.03}Te$ are 2.04 and 1.30 m_0 (SPB mode), respectively. The η of both In-doped and Bi-doped samples are in the region where both LVB and HVB actively participate in the electronic transport. One difference between the In-doped and Bi-doped samples is the location of their η relative to the HVB maximum. The η of the In-doped sample is slightly below the HVB maximum, indicating that the HVB is the major band. The η of the Bi-doped sample is above the HVB maximum, indicating that the LVB is the major band in the sample. The difference in the major band affects the resulting m_d^* estimated by the SPB model. For example, the m_d^* of the In-doped sample is heavier than that of the pristine SnTe due to the additional resonant state formation effect, but the m_d^* of the Bi-doped sample is lighter than the pristine SnTe even with the resonant state. The m_d^* of the pristine SnTe and $Sn_{0.97}M_{0.03}Te$ (M = Ga, In, Bi, and Sb) obtained by using the SPB model are closely related to the electronic band structure incorporated in the TB model as shown in Figure 1(c). Therefore, the SPB model is an effective tool for understanding the effect of electron doping and resonant state formation.

Figure 2(c) shows the temperature-dependent m_d^* calculated for the pristine SnTe and $Sn_{0.97}M_{0.03}Te$ (M = Ga, In, Bi, and Sb) using the SPB model. The band structure provided in Figure 1(c) for the pristine SnTe can be changed with doping or temperature [31]. For example, the m_d^* increase with an increasing temperature observed in the pristine SnTe is related to the possible change in the ΔE between the LVB and HVB at high temperatures. This increase in m_d^* with temperature is also observed in Ga-doped and Sb-doped samples. However, the m_d^* of the In-doped sample at 823 K (1.96 m_0) is lighter than that calculated at 300 K (2.04 m_0). This shows that the effect of resonant state formation only observed at 300 K is stronger than the LVB and HVB converging in energy at high temperatures [32]. On the contrary, the m_d^* of the Bi-doped SnTe at 300 K (1.30 m_0) is lighter than that obtained at 823 K (1.63 m_0). The convergence of the LVB and HVB at high temperatures due to Bi doping has a larger impact on the band structure than the resonant state formed by Bi doping near 300 K.

Figure 3(a) shows the experimental and calculated μ_H as a function of n_H at 300 K [14]. By fitting Equations (3) and (4) to the measurements (in filled symbols), the calculated n_H-dependent μ_H (in lines) are calculated. For the m_d^* in Equation (5), the m_d^* obtained in Figure 2 are used. Experimental μ_H of the pristine SnTe (34 cm^2 s^{-1} V^{-1}) is the lowest among other doped SnTe samples at 300 K. As the n_H decreases with electron doping, the corresponding μ_H significantly increases. For example, the μ_H of In-doped sample is approximately 44 cm^2 s^{-1} V^{-1}, which almost doubles to 87 cm^2 s^{-1} V^{-1} in the Bi-doped sample. Moreover, the μ_H of Sb-doped sample amounts to 539 cm^2 s^{-1} V^{-1}. However, the μ_0 obtained from the measurements do not necessarily follow the trend of the experimental μ_H. This is because μ_0 is the mobility of the sample when the sample is defectless and its n_H is close to its nondegenerate regime.

In Figure 3(b), the μ_0 used to calculate the theoretical n_H-dependent μ_H at 300 K (Figure 3(b) in lines) are presented for the pristine SnTe and doped SnTe samples. The μ_0 of pristine SnTe is 107 cm^2 s^{-1} V^{-1}, and when SnTe is

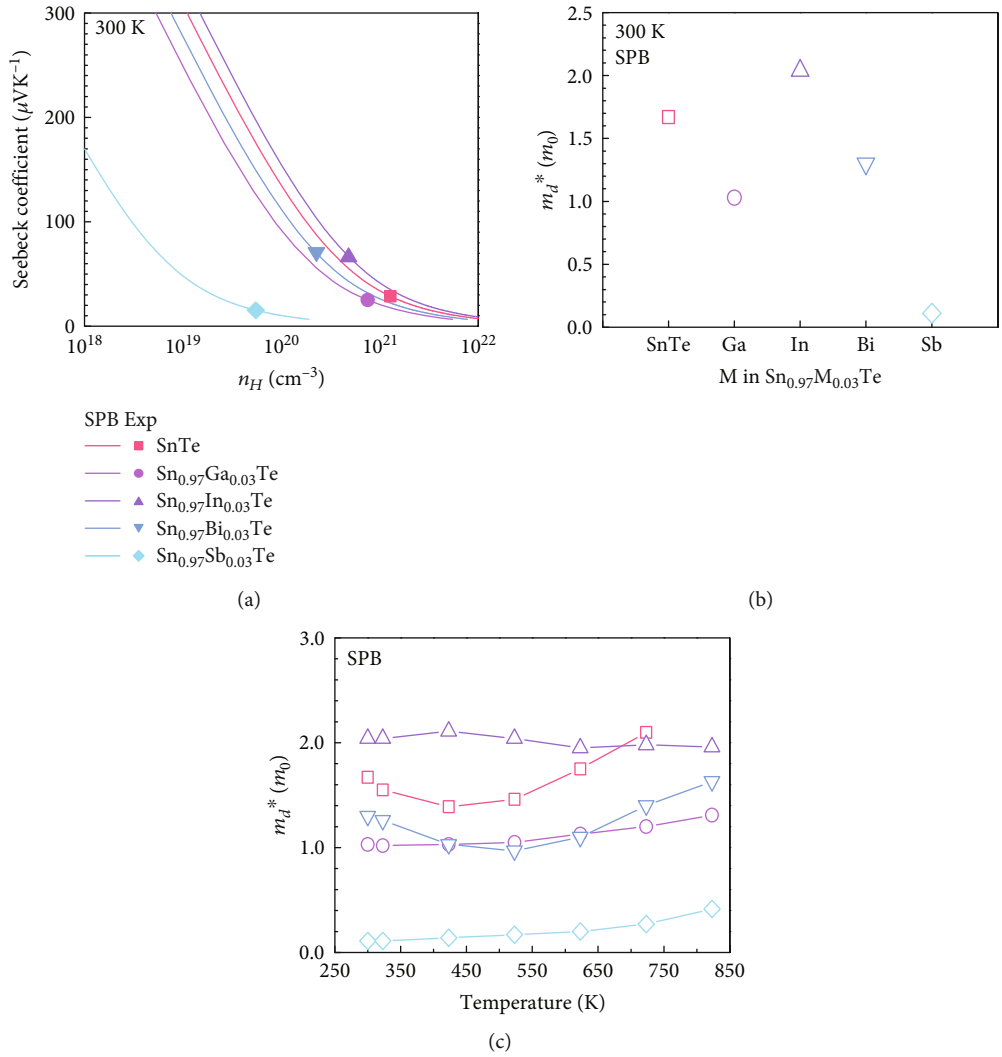

FIGURE 2: (a) The experimental (in filled symbols) [14] and calculated (in lines) S with varying n_H, (b) the fitted m_d^* at 300 K (empty symbols), and (c) temperature-dependent m_d^* for pristine SnTe and $Sn_{0.97}M_{0.03}Te$ (M = Ga, In, Bi, Sb) using the SPB model (empty symbols).

doped with Ga, In, Bi, and Sb, the μ_0 is calculated to be 136, 92, 182, and 2320 $cm^2 s^{-1} V^{-1}$, respectively. Because the μ_0 is a band parameter, its value estimated by the SPB model is also affected by the position of the η in the band structure (Figure 1(c)). The η of the pristine SnTe, Ga-doped, and In-doped SnTe are positioned at the HVB. On the contrary, the η of the Bi-doped and Sb-doped samples are placed at the LVB. Because the μ_0 is inversely proportional to the m_d^*, the μ_0 of the Bi-doped and Sb-doped samples, whose major band in the LVB, are higher than those of other samples. The reason that the μ_0 of the Sb-doped sample (2320 $cm^2 s^{-1} V^{-1}$) is much higher than that of the Bi-doped sample (182 $cm^2 s^{-1} V^{-1}$) is that the contribution from the HVB is almost negligible in the Sb-doped sample. When Figure 3(b) is compared to Figure 2(b), we can see that the trend of the μ_0 change with different dopants (Figure 2(b)) is opposite to the trend of the m_d^* change (Figure 3(b)). For example, In doping decreases the μ_0 of SnTe while increasing the m_d^* when compared to those of the pristine SnTe. If the decrease in μ_0 is less than expected from the m_d^* increase, we can suspect that band engineering is applied to overcome the S-σ trade-off relation. In order to closely evaluate the effect of resonant state formation or change in ΔE between the LVB and HVB, the μ_W needs to be characterized, which is an m_d^*-weighted μ_0 (Equation (5)).

Figure 3(c) shows the calculated μ_0 as a function of temperature. All samples exhibit a decreasing trend in μ_0 as the temperature increases. The decrease in μ_0 is mostly due to the increased carrier-phonon interaction at high temperatures. The carrier-phonon interaction is expressed as a deformation potential (Ξ), and it is also inversely proportional to μ_0. In addition, Zhou et al. reported that the m_d^* of the LVB and HVB decreased at high temperatures [25]. The decreases in Ξ and m_d^* are the primary reasons for the μ_0 decrease with temperature. Different samples have different rates of μ_0 decrease with an increasing temperature. The temperature coefficient of μ_0 for the pristine SnTe and doped SnTe are shown in Table 2.

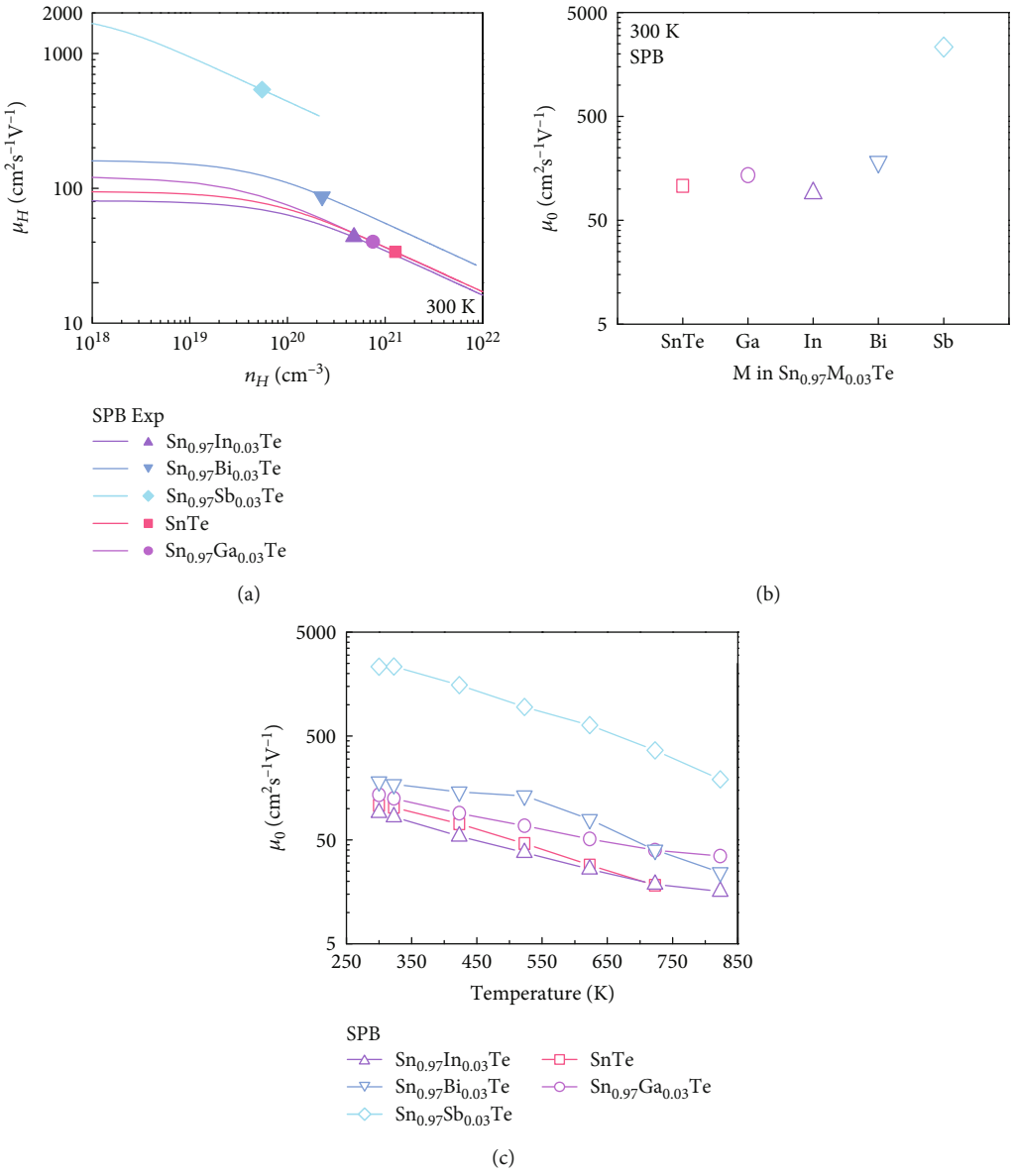

FIGURE 3: (a) The experimental (in filled symbols) [14] and calculated (in lines) μ_H with varying n_H, (b) the fitted μ_0 at 300 K (empty symbols), and (c) temperature-dependent μ_0 for pristine SnTe and $Sn_{0.97}M_{0.03}Te$ (M = Ga, In, Bi, Sb) using the SPB model (empty symbols).

The temperature coefficient of μ_0 ($\Delta\mu_0/\Delta T$) is calculated by Equation (16) below.

$$\frac{\Delta\mu_0}{\Delta T} = \frac{\mu_{0,823K} - \mu_{0,300K}}{523\,K}. \quad (16)$$

The $\mu_{0,823K}$ and $\mu_{0,300K}$ are the μ_0 at 823 K and that at 300 K, respectively. Because the Bi-doped does not have the μ_0 at 823 K, $\mu_{0,723K}$ is used instead with ΔT of 423 K. The $\Delta\mu_0/\Delta T$ of the pristine SnTe, Ga-doped, and In-doped SnTe samples, whose η are initially at the HVB at 300 K, are lower than those calculated in the Bi-doped and Sn-doped samples. As the η increases with Ga and In dopings, corresponding $\Delta\mu_0/\Delta T$ decrease. However, for the Bi-doped and Sb-doped samples, whose η are initially at the LVB at 300 K, the decrease in η (from Bi-doped to Sb-doped sample) significantly increases the $\Delta\mu_0/\Delta T$ (by more than 13 times in magnitude). Physical mechanism behind the observed $\Delta\mu_0/\Delta T$ is not straightforward as it is correlated to the temperature

TABLE 2: The temperature coefficient of μ_0 for the pristine SnTe and $Sn_{0.97}M_{0.03}Te$ (M = Ga, In, Bi, Sb).

Dopant	Temperature coefficient of μ_0 (cm^2 s^{-1} V^{-1} K^{-1})
Pristine	-0.21
Ga	-0.19
In	-0.14
Bi	-0.30
Sb	-4.08

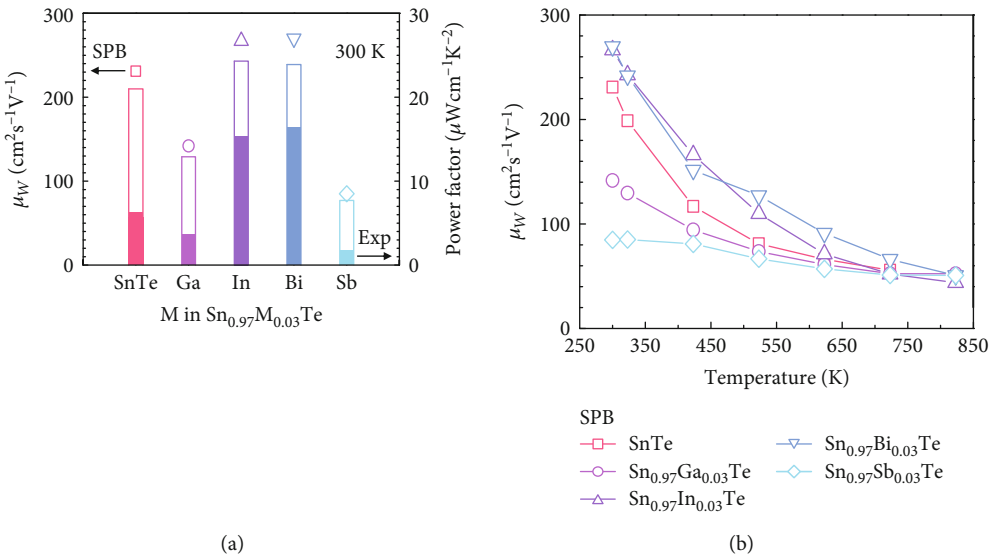

(a) (b)

FIGURE 4: (a) μ_W (in symbols), experimental *PF* (in filled bars) [14], theoretical maximum *PF* (in empty bars) at 300 K, and (b) temperature-dependent μ_W for pristine SnTe and $Sn_{0.97}M_{0.03}Te$ (M = Ga, In, Bi, and Sb).

coefficients of m_d^* and Ξ for both LVB and HVB and to how the ΔE between the LVB and HVB changes with an increasing temperature. Nonetheless, it is important to note that the $\mu_{0,823K}$ of the Sb-doped sample is the highest, because this result hints that the η should be placed in the LVB for the higher thermoelectric performance.

Figure 4(a) shows μ_W at 300 K calculated by substituting m_d^* (Figure 2(b)) and μ_0 (Figure 3(b)) into Equation (5) [18]. The μ_W is a better indicator of band engineering than the m_d^* alone. This means that the μ_W can be used to identify a wider range of band engineering effects, including band convergence and resonant state formation. The μ_W of In-doped and Bi-doped samples ($\geq 267\,cm^2\,s^{-1}\,V^{-1}$) are higher than those of other samples ($\leq 231\,cm^2\,s^{-1}\,V^{-1}$) at 300 K. The high μ_W of In-doped and Bi-doped samples can be attributed to the resonant state formation as confirmed in Figure 1(a). The m_d^* of the Bi-doped sample ($1.30\,m_0$) was lighter than that of the pristine sample ($1.67\,m_0$) in Figure 2(a). However, when the μ_W is considered, we see that the μ_W of the Bi-doped sample ($270\,cm^2\,s^{-1}\,V^{-1}$) is higher than that of the pristine SnTe ($231\,cm^2\,s^{-1}\,V^{-1}$) by approximately 17%. The filled bars in Figure 4(a) show the experimental *PF* reported at 300 K [14]. The experimental *PF* is positively correlated with the μ_W of a sample. This means that as the μ_W of a sample increases, the *PF* of the sample also tends to increase. The experimental *PF* of the Bi-doped sample is the highest among all the samples, with a value of $158\,\mu W\,cm^{-1}\,K^{-2}$. This is consistent with the fact that the μ_W of the Bi-doped sample is also the highest ($270\,cm^2\,s^{-1}\,V^{-1}$). The theoretical maximum *PF* is directly proportional to the μ_W, while the experimental *PF* is not. This means that the μ_W can only be used to predict the theoretical maximum *PF*, and not the actual experimental *PF*. The theoretical maximum *PF* predicted by the SPB model (using the μ_W in Figure 4(a)) is presented in empty bars. According to the SPB model, the *PF* of the Bi-doped sample can be further improved by more than 51.3% ($15.8 \longrightarrow 23.9\,\mu W\,cm^{-1}\,K^{-2}$) after appropriate n_H tuning.

Figure 4(b) shows the calculated μ_W as a function of temperature. All samples show a decrease in μ_W as temperature increases, with the decrease rate being the smallest for the Sb-doped sample. The temperature coefficient of m_d^* is much smaller than the temperature coefficient of μ_0, making it insignificant. Therefore, the decrease in μ_W with an increasing temperature mostly stems from the temperature coefficient of μ_0 (Figure 3(c)). The μ_W of the Ga-doped ($52\,cm^2\,s^{-1}\,V^{-1}$), Bi-doped ($51\,cm^2\,s^{-1}\,V^{-1}$), and Sb-doped samples ($51\,cm^2\,s^{-1}\,V^{-1}$) are the highest at 823 K, with values that are higher than the other samples. The μ_W of the Sb-doped sample is the lowest at 300 K, but it increases sharply at higher temperatures. This is noteworthy because it suggests that placing the η at the LVB at 300 K may be a promising way to improve the thermoelectric properties of materials at high temperatures. The μ_W of the Bi-doped sample, which is the highest at 300 K, remains high even at 823 K, which further supports this hypothesis.

Figure 5(a) shows the calculated *B*-factor of for the pristine SnTe and $Sn_{0.97}M_{0.03}Te$ (M = Ga, In, Bi, and Sb) at 300 K. The *B*-factor is calculated through Equation (6) using the calculated μ_W (Figure 4(a)) and the measured κ_l [14]. The measured κ_l of the pristine and doped SnTe are given in Figure 5(b). According to Equation (6), the *B*-factor is directly proportional to the ratio of the μ_W to κ_l. The trend in the *B*-factor is similar to that in the μ_W for the doped SnTe samples (Figure 4(a)). This is because the κ_l of all the doped samples is similar ($\sim 1.9\,W\,m^{-1}\,K^{-1}$). Because all the doped samples are doped with the same doping content (3.0 at.%), the κ_l of the doped samples being comparable is reasonable. Despite its much higher μ_W of $231\,cm^2\,s^{-1}\,V^{-1}$ than the Ga-doped sample ($142\,cm^2\,s^{-1}\,V^{-1}$), the *B*-factor of pristine SnTe (0.047) becomes comparable to that of the Ga-doped sample (0.049). This is because the pristine SnTe

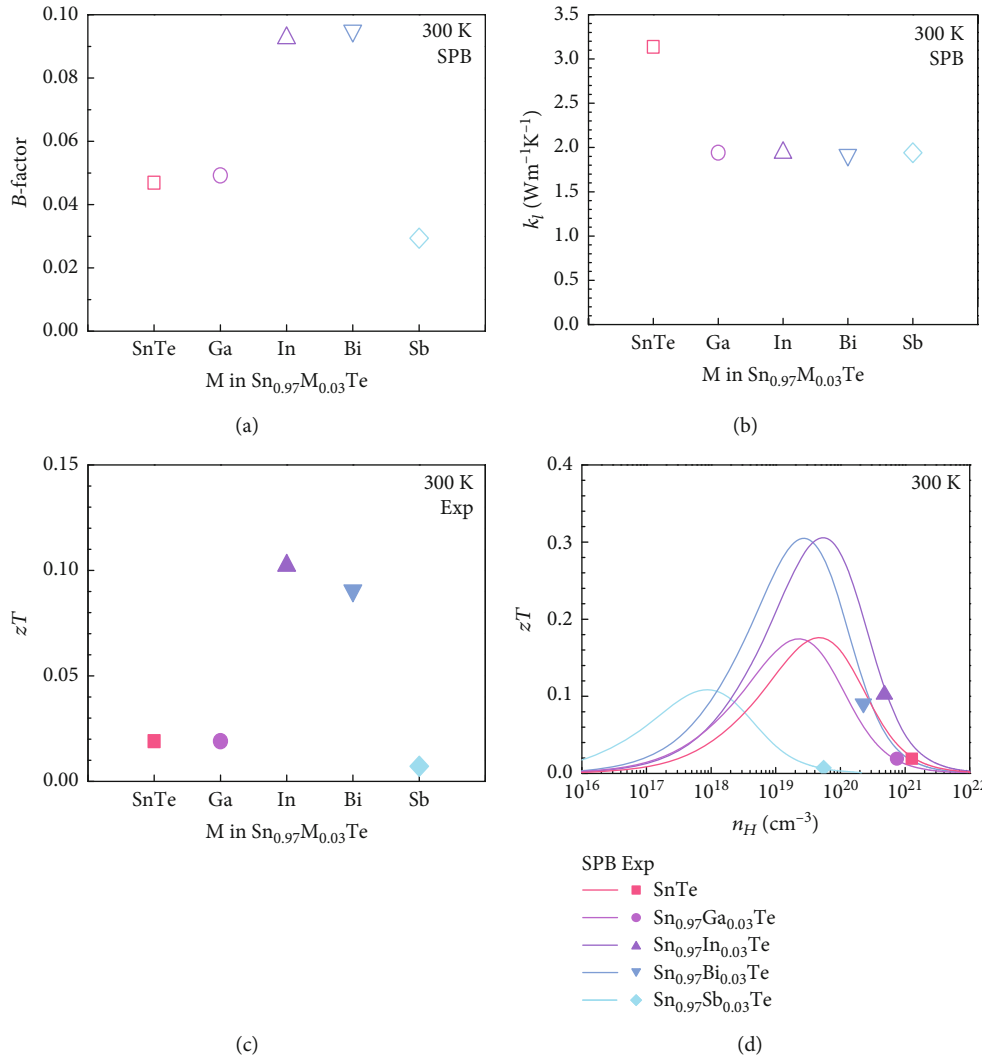

FIGURE 5: (a) Calculated B-factor, (b) experimental κ_l, (c) zT [14], and (d) experimental and calculated n_H-dependent zT for the pristine SnTe and $Sn_{0.97}M_{0.03}Te$ (M = Ga, In, Bi, and Sb) at 300 K.

has a much higher thermal conductivity κ_l (3.1 $W\,m^{-1}\,K^{-1}$) than the Ga-doped sample (1.9 $W\,m^{-1}\,K^{-1}$). The B-factor is a measure of intrinsic band and phonon transport properties, and it is related to the theoretical maximum zT. However, the B-factor is not directly proportional to the theoretical maximum zT. The Bi-doped sample has the highest B-factor (0.095) among the pristine and doped SnTe samples at 300 K. This suggests that the zT of the Bi-doped sample can be the highest at 300 K when the n_H is optimized.

Figure 5(c) shows the experimental zT of the pristine and doped SnTe at 300 K [14]. Here, the zT of the In-doped sample (zT~0.10) is slightly higher than the Bi-doped sample (0.09). However, based on the B-factor calculated in Figure 5(a), the zT of the Bi-doped sample can be higher than that of the In-doped if its n_H is tuned optimally. Figure 5(d) shows the n_H -dependent zT of the pristine and doped SnTe samples at 300 K. The experimental results are plotted in filled symbols, and the calculated results (SPB model) are presented in solid lines. Most of the pristine and doped samples have their theoretical maximum zTs at n_H higher than $10^{19}\,cm^{-3}$. We have approximated the contributions from the LVB, HVB, and the resonant state of electron-doped SnTe samples with the SPB model and predicted their maximum zT and optimum n_H. While the SPB model may not produce a perfectly accurate prediction, the error is likely to be small. Thus, the n_H -depedent zT predicted by the SPB model can serve as a useful guide for experimentalists in tuning n_H. Additionally, the prediction error in the SPB model decreases as the n_H increases (when the Fermi level is deep within the HVB, where the discrepancy between the SPB model and the TB model is minimized). In other words, except for Sb-doped SnTe, which has the lowest n_H, other electron-doped SnTe samples with high n_H would have their n_H-dependent zT accurately predicted by the SPB model. However, the zT of the Sb-doped sample is estimated to be at its maximum near $10^{18}\,cm^{-3}$. This has to do with the η of the Sb-doped sample being at the LVB with a negligible effect from the HVB (Figure 1(c)). On the contrary, the theoretical zT of the Bi-doped sample peaks at

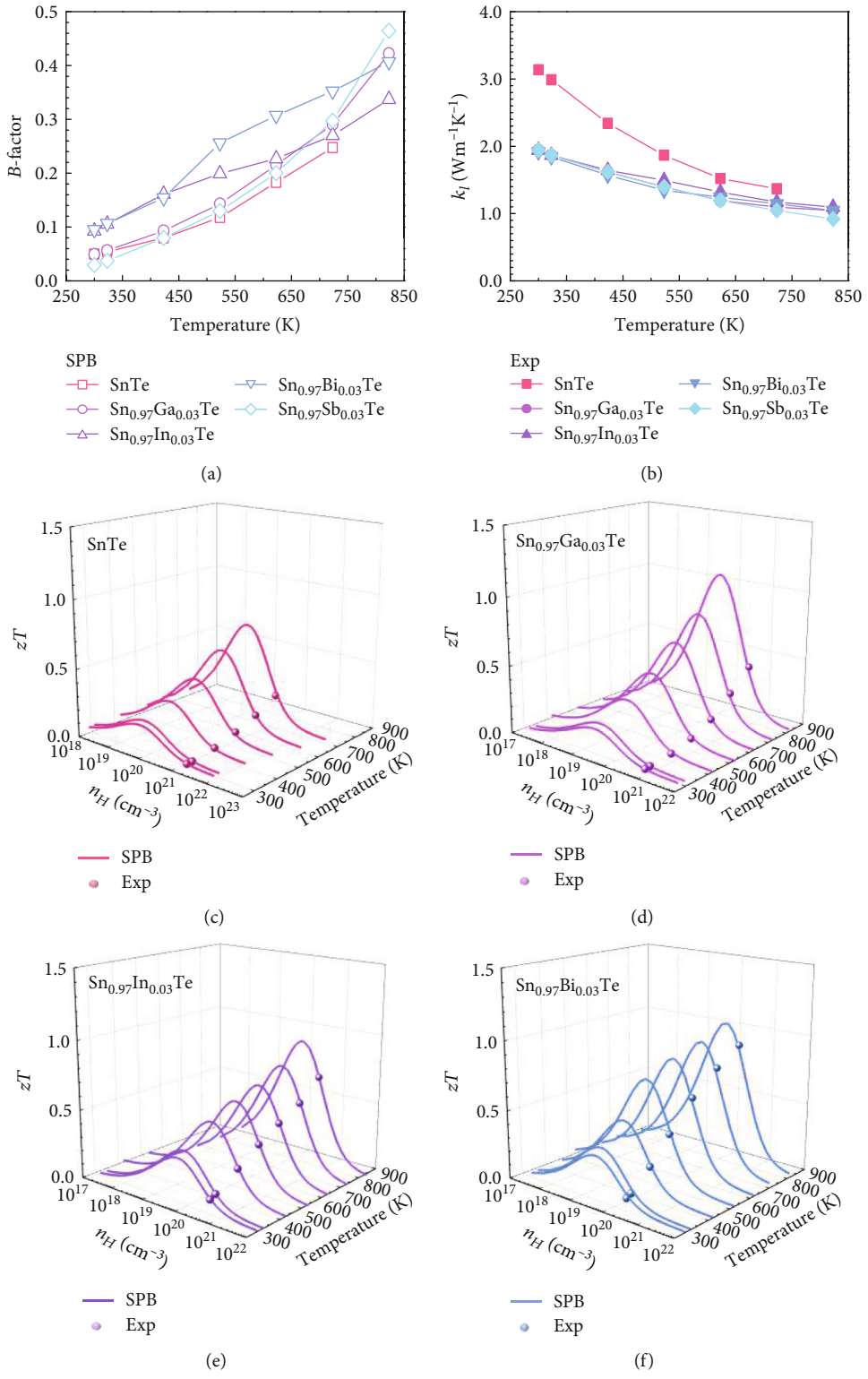

Figure 6: Continued.

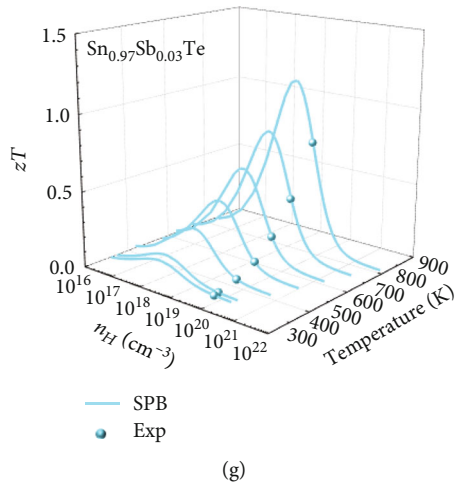

FIGURE 6: Temperature-dependent (a) B-factor estimations, (b) κ_l measurements [14], and (c–g) zT estimations (in lines) and measurements (in symbols) for varying n_H for the pristine and SnTe and $Sn_{0.97}M_{0.03}Te$ (M = Ga, In, Bi, and Sb).

3.7×10^{19} cm^{-3}, even though its η is at the LVB. In this case, the HVB maximum adjacent to the η of the Bi-doped sample is responsible for the difference. Based on the SPB model, the theoretical maximum zT of the Bi-doped sample (zT~0.311) is lower than that of the In-doped sample (0.312). This is as predicted from the calculated B-factor in Figure 5(a). The significantly higher theoretical maximum zTs of the In-doped and Bi-doped samples than those of other samples can be attributed to the formation of the resonant states. For the Bi-doped sample, its zT can be improved by ~244% (0.09⟶0.31) when the n_H is tuned to 3.7×10^{19} cm^{-3}.

Figures 6(a) and 6(b) show the calculated B-factor and measured κ_l as a function of temperature. The B-factor in Figure 6(a) is calculated by using the temperature-dependent μ_W (Figure 4(b)) and κ_l (Figure 6(b)). The B-factor of all the samples increases with an increasing temperature. This is because the κ_l decreases as the temperature increases and the B-factor scales with $T^{5/2}$ (Equation (6)). From the fact that the B-factor increases with temperature, we can predict that the theoretical maximum zT of the pristine and doped SnTe will increase with temperature. The temperature-dependent B-factor in Figure 6(a) has two interesting observations. Firstly, the samples with their η at the HVB (nonshaded region in Figure 1(c)) or LVB (shaded in blue in Figure 1(c)) with negligible contribution from other bands have a low B-factor at low temperatures (pristine; Ga-doped and Sb-doped samples). However, the rate of B-factor increase with temperature is high for these samples. So the B-factors of the Sb-doped (0.46) and Ga-doped samples (0.41) become the highest and the second highest among all the samples at 823 K. Secondly, the In-doped and Bi-doped samples whose η is at the region where both HVB and LVB contribute (shaded in light blue in Figure 1(c)) have high B-factor until ~700 K. Their high B-factor near 300 K is due to the resonant state formation. The rate of B-factor increase with temperature for the Bi-doped sample suddenly increases near 550 K while that of the In-doped sample decreases. As the temperature increases, contribution from another band adjacent in energy increases. For the Bi-doped sample, the contribution from the HVB increases with temperature, while for the In-doped sample, the contribution from the LVB increases with temperature. Therefore, it is advantageous to place the η at LVB at 300 K for the improved thermoelectric performance at higher temperatures. The highest experimental zT of ~0.9 at 823 K for the Bi-doped sample can be attributed to the following factors: the resonant state formation at 300 K, the position of the η in the region where both the LVB and HVB contribute to transport, and the fact that η is actually on the LVB and not the HVB. From the highest B-factor of the Sb-doped sample at 823 K, we expect the highest theoretical maximum zT in the Sb-doped sample. However, even when the n_H is optimally tuned, the average zT of the Bi-doped sample will be higher than that of the Sb-doped sample as the B-factor of the Sb-doped sample is only higher than that of the Bi-doped sample at temperatures higher than 823 K.

Figures 6(c)–6(g) show the experimental (in symbols) and calculated zT (in lines) as a function of n_H and temperature. A comparison of the experimental n_H and calculated optimum n_H for the maximum zT at a specific temperature can be used as a guide for further zT improvement. The theoretical maximum zT of the Sb-doped sample (zT~1.13) at 823 K is the highest followed by the Ga-doped (1.06) and Bi-doped samples (1.03). However, even when the n_H is optimized, the average zT, which is more important for the efficiency of the thermoelectric device, will be the highest in the Bi-doped sample because of the steady increase in the theoretical maximum zT over the whole temperature range. Another 14% increase in the zT of the Bi-doped sample (0.9⟶1.03) is possible at 823 K if the n_H is tuned. Additionally, a more than 61% increase in the zT is also possible in the Sb-doped sample (0.7⟶1.13). For the highest zT at high temperature, the η should be placed at one of the valence bands where the contribution from the other band is not strong at 300 K. To achieve the highest zT at high temperature, the η should be placed in a valence band where the contribution from the other band is not strong at 300 K. However, to achieve the highest average zT, placing η at the LVB near the HVB maximum is advantageous.

4. Conclusion

In summary, we evaluated the effect of electron doping in p-type SnTe using Ga, In, Bi, and Sb as dopants ($Sn_{0.97}M_{0.03}Te$ (M = Ga, In, Bi, Sb)) using the two-band (TB) and single parabolic band (SPB) models. We found that In-doped and Bi-doped samples formed the resonant states near 300 K because their experimental data significantly deviated from the Hall carrier concentration (n_H)-dependent Seebeck coefficient (S) calculated using the TB model (one light valence band (LVB) and a heavy valence band (HVB) participating in electronic transport). We also identified where the Fermi levels (η) of the doped samples are positioned. The η of the Sb-doped sample was at the LVB while that of the Ga-doped sample was at the HVB further apart from the maximum of the other band. However, the η of both In-doped and Bi-doped samples were in the region where both LVB and HVB are active. We then estimated the band parameters such as weighted mobility (μ_W) and B-factor of the doped samples using the SPB model as a function of temperature. According to the temperature-dependent B-factor, which is related to the theoretical maximum zT, the In-doped and Bi-doped samples with the resonant state formation near 300 K and their η positioned where both the LVB and HVB participate in transport exhibited high average zT than other samples. Especially, the Bi-doped sample whose η was at the LVB had the higher theoretical maximum zT (zT~1.03) than the In-doped sample (0.90) at 823 K. Choosing a dopant that forms a resonant state at 300 K and engineering the position of η so that it is at the LVB but still close to the HVB maximum are important strategies for achieving a high average zT in SnTe.

Data Availability

Data are available upon request.

Conflicts of Interest

There is no conflict of interest.

Authors' Contributions

Hyunjin Park, Kyu Hyoung Lee, and Minsu Heo contributed equally to this work.

Acknowledgments

This research was supported by the Nano·Material Technology Development Program through the National Research Foundation of Korea (NRF) funded by the Ministry of Science and ICT (2022M3H4A1A04076667). This work was also supported by the National Research Foundation of Korea (NRF) grant funded by the Korea government (MSIT) (RS-2023-00212959).

References

[1] J. R. Sootsman, D. Y. Chung, and M. G. Kanatzidis, "New and old concepts in thermoelectric materials," *Angewandte Chemie International Edition*, vol. 48, no. 46, pp. 8616–8639, 2009.

[2] H. Park, S. Kim, K. Lee, W. S. Seo, and H. S. Kim, "Effects of Ti doping on TaFeSb half-Heuslers estimated by a single parabolic band model," *ChemNanoMat*, vol. 8, no. 11, article e202200370, 2022.

[3] J. Yang, G. Meisner, and L. Chen, "Strain field fluctuation effects on lattice thermal conductivity of ZrNiSn -based thermoelectric compounds," *Applied Physics Letters*, vol. 85, no. 7, pp. 1140–1142, 2004.

[4] G. Kim, S. W. Kim, H. J. Rim et al., "Improved trade-off between thermoelectric performance and mechanical reliability of Mg_2Si by hybridization of few-layered reduced graphene oxides," *Scripta Materialia*, vol. 162, pp. 402–407, 2019.

[5] H. Park, S. Kim, J. Y. Kim, S. M. Hwang, and H. S. Kim, "Estimation of temperature-dependent band parameters for bi-doped SnSe with high thermoelectric performance," *Ceramics*, vol. 6, no. 1, pp. 504–513, 2023.

[6] T. M. Tritt, *Thermal Conductivity: Theory, Properties, and Applications; Physics of Solids and Liquids*, Springer, Boston, 2006.

[7] G. Tan, F. Shi, S. Hao et al., "Codoping in SnTe: enhancement of thermoelectric performance through synergy of resonance levels and band convergence," *Journal of the American Chemical Society*, vol. 137, no. 15, pp. 5100–5112, 2015.

[8] H. Kim, N. A. Heinz, Z. M. Gibbs, Y. Tang, S. D. Kang, and G. J. Snyder, "High thermoelectric performance in $(Bi_{0.25}Sb_{0.75})_2Te_3$ due to band convergence and improved by carrier concentration control," *Materials Today*, vol. 20, no. 8, pp. 452–459, 2017.

[9] M. Heo, S. H. Kwon, S. I. Kim, H. Park, K. H. Lee, and H. S. Kim, "Impact of resonant state formation and band convergence in In and Sr co-doped SnTe thermoelectric material evaluated via the single parabolic band model," *Journal of Alloy and Compounds*, vol. 954, article 170144, 2023.

[10] W. Li, S. Lin, M. Weiss et al., "Crystal structure induced ultralow lattice thermal conductivity in thermoelectric Ag_9AlSe_6," *Advanced Energy Materials*, vol. 8, no. 18, 2018.

[11] G. Tan, L. Zhao, F. Shi et al., "High thermoelectric performance of p-type SnTe via a synergistic band engineering and nanostructuring approach," *Journal of the American Chemical Society*, vol. 136, no. 19, pp. 7006–7017, 2014.

[12] Y. Zhang, J. Li, W. Hu, X. Yang, X. Tang, and G. Tan, "Boosting thermoelectric performance of SnTe by selective alloying and band tuning," *Materials Today Energy*, vol. 25, article 100958, 2022.

[13] D. K. Bhat and U. S. Shenoy, "SnTe thermoelectrics: dual step approach for enhanced performance," *Journal of Alloys and Compounds*, vol. 834, article 155181, 2020.

[14] L. Zhao, X. Zhang, H. Wu et al., "Enhanced thermoelectric properties in the counter-doped SnTe system with strained endotaxial SrTe," *Journal of the American Chemical Society*, vol. 138, no. 7, pp. 2366–2373, 2016.

[15] A. Banik, S. Shenoy, S. Anand, U. V. Waghmare, and K. Biswas, "Mg alloying in SnTe facilitates valence band convergence and optimizes thermoelectric properties," *Chemistry of Materials*, vol. 27, no. 2, pp. 581–587, 2015.

[16] G. Tan, F. Shi, J. W. Doak et al., "Extraordinary role of Hg in enhancing the thermoelectric performance of p-type SnTe," *Energy & Environmental Science*, vol. 8, no. 1, pp. 267–277, 2015.

[17] G. Tan, F. Shi, S. Hao et al., "Valence band modification and high thermoelectric performance in SnTe heavily alloyed with MnTe," *Journal of American Chemical Society*, vol. 137, no. 35, pp. 11507–11516, 2015.

[18] H. Wang, Y. Pei, A. D. LaLonde, and G. Jeffery Snyder, "Material Design Considerations Based on Thermoelectric Quality Factor," in *Thermoelectric Nanomaterials. Springer Series in Materials Science*, K. Koumoto and T. Mori, Eds., vol. 182, Springer, Berlin, Heidelberg, 2013.

[19] J.-C. Lim, S. Y. Kim, W. H. Shin et al., "Characterization of hall factor with Seebeck coefficient measurement," *ACS Applied Energy Materials*, vol. 5, no. 4, pp. 4036–4040, 2022.

[20] M. Hirschberger, J. W. Krizan, R. J. Cava, and N. P. Ong, "Large thermal hall conductivity of neutral spin excitations in a frustrated quantum magnet," *Science*, vol. 348, no. 6230, pp. 106–109, 2015.

[21] K. H. Lee, Y.-M. Kim, C. O. Park et al., "Cumulative defect structures for experimentally attainable low thermal conductivity in thermoelectric $(Bi,Sb)_2Te_3$ alloys," *Materials Today Energy*, vol. 21, article 100795, 2021.

[22] M. Kim, S. Kim, S. W. Kim, H. Kim, and K. H. Lee, "Weighted mobility ratio engineering for high-performance Bi–Te-based thermoelectric maiterials via suppression of minority carrier transport," *Advanced Materials*, vol. 33, no. 47, 2021.

[23] G. J. Snyder, A. H. Snyder, M. Wood, R. Gurunathan, B. H. Snyder, and C. G. J. Niu, "Weighted mobility," *Advanced Materials*, vol. 32, no. 25, 2020.

[24] Q. Zhang, B. Liao, Y. Lan et al., "High thermoelectric performance by resonant dopant indium in nanostructured SnTe," *Proceedings of the National Academy of Sciences*, vol. 110, no. 33, pp. 13261–13266, 2013.

[25] M. Zhou, Z. M. Gibbs, H. Wang et al., "Optimization of thermoelectric efficiency in SnTe: the case for the light band," *Physical Chemistry Chemical Physics*, vol. 16, no. 38, pp. 20741–20748, 2014.

[26] Z. Zhou, J. Yang, Q. Jiang et al., "Multiple effects of Bi doping in enhancing the thermoelectric properties of SnTe," *Journal of Materials Chemistry A*, vol. 4, no. 34, pp. 13171–13175, 2016.

[27] V. P. Vedeneev, S. P. Krivorruchko, and E. P. Sabo, "Tin telluride based thermoelectrical alloys," *Semiconductors*, vol. 32, no. 3, pp. 241–244, 1998.

[28] M. O. Galushchak, D. M. Freik, I. M. Ivanyshyn, A. V. Lisak, and M. V. Pyts, "Thermoelectric properties and defective subsystem in doped telluride of tin," *Journal of Thermoelectricity*, vol. 20, no. 2, pp. 149–155, 2000.

[29] U. S. Shenoy and D. K. Bhat, "Bi and Zn co-doped SnTe thermoelectrics: interplay of resonance levels and heavy hole band dominance leading to enhanced performance and a record high room temperatureZT," *Journal of Materials Chemistry C*, vol. 8, no. 6, pp. 2036–2042, 2020.

[30] U. S. Shenoy and D. K. Bhat, "Electronic structure engineering of tin telluride through co-doping of bismuth and indium for high performance thermoelectrics: a synergistic effect leading to a record high room temperatureZTin tin telluride," *Journal of Materials Chemistry C*, vol. 7, no. 16, pp. 4817–4821, 2019.

[31] M. Zhou, G. J. Snyder, L. Li, and L.-D. Zhao, "Lead-free tin chalcogenide thermoelectric materials," *Inorganic Chemstry Frontiers*, vol. 3, no. 11, pp. 1449–1463, 2016.

[32] G. Tan, W. G. Zeier, F. Shi et al., "High thermoelectric performance SnTe–In2Te3Solid solutions enabled by resonant levels and strong vacancy phonon scattering," *Chemistry of Materials*, vol. 27, no. 22, pp. 7801–7811, 2015.